COELACANTH-SCALE INSPIRED THIN-PLY COMPOSITES FOR BEARING APPLICATIONS

Marcel Neubacher[1], Farida Touni[1] and Bodo Fiedler[1]

[1]Institute of Polymers and Composites (IPC), Hamburg University of Technology (TUHH),
Denickestraße 15, D-21073 Hamburg, Germany
Web Page: https://www.tuhh.de/kvweb/en/home
Email: marcel.neubacher@tuhh.de
Email: farida.touni@ tuhh.de
Email: fiedler@tuhh.de

Keywords: Bio-Inspired, Bouligand, CFRP, Notch sensitivity, CLT

Abstract
Thin-ply composites are known for their superior in-situ strength and manufacturing quality, offering higher unnotched tensile and compressive strengths compared to conventional laminates. However, their damage suppression capability leads to increased notch sensitivity, where delamination and matrix cracking mechanisms are suppressed. As a result, thin-ply laminates are limited in their use in critical load-bearing applications.To address this, bio-inspired Bouligand structures, defined by their helical fiber arrangements, have shown promise in reducing notch sensitivity through helicoidal matrix cracking and stress redistribution. This study explores the mechanical performance of partial Bouligand layups derived from biological fiber architectures observed in coelacanth fish scales, where fibrils reorient under load [1]. An analytical stiffness based optimization was performed to match the mechanical properties of the conventional [0 °, ±45 °, 90 °] (50 %, 40 %, 10 %) load introduction layup used in bolted and riveted aircraft structures [2, 3], while integrating the partial Bouligand structure.Two layer fiber areal weights (30 gsm and 60 gsm) were investigated, resulting in different pitch and stack angles. Tensile and bearing tests were conducted to evaluate the influence of the partial Bouligand structure on notch sensitivity. The results indicate that nature inspired fiber orientation can improve load redistribution and damage tolerance in thin ply laminates, making them compatible for off-axis and notched applications.

1. Introduction

Thin-ply carbon fiber reinforced polymers (CFRPs), produced using techniques such as spread-tow processes, have emerged as a high-performance alternative to conventional composites, with individual ply thicknesses reaching as low as 20 µm [4]. The reduction in ply thickness enables greater design flexibility by increasing the number of plies within a laminate and allowing for more precise tailoring of fiber orientations based on load paths.
Thin plies also demonstrate superior in-situ strength, suppressing mechanisms such as transverse microcracking and free-edge delamination. This leads to a transition in failure behavior from delamination-dominated modes in thick plies to more brittle, fiber-dominated failure in thin plies, resulting in higher ultimate tensile and compressive strengths in unnotched quasi-isotropic and unidirectional laminates. In addition to improved mechanical performance,

thin-ply laminates benefit from enhanced manufacturing quality, including lower void content, better fiber alignment, and reduced resin-rich zones. [5]
However, despite these advantages, thin-ply laminates often exhibit heightened notch sensitivity, particularly in tension, which can lead to a premature and brittle failure when stress concentrations, such as holes or impact damage are introduced. Thin-ply laminates tend to exhibit lower ultimate open hole tensile (OHT) strength, up to 30 % less than thick plies, as they suppress damage mechanisms like delamination and inter-fiber cracking, which conventionally help redistribute stress around notches [6, 7]. This results in pronounced notch sensitivity, where the composite's strength and stiffness drop sharply near stress concentrators, reducing the effective load the structure can safely carry. To address this challenge, structural modifications that reintroduce controlled damage mechanisms have been proposed. Among the most promising approaches are bio-inspired fiber architectures, such as Bouligand (helicoidal) layups, which gradually rotate fiber orientations between adjacent plies [8, 9].
Bouligand composites demonstrate superior performance and damage tolerance under OHT loading compared to both quasi-isotropic (QI) and traditional cross-ply laminates. As shown in [9], thin-ply Bouligand structures with extremely low pitch angles, mimic biological fiber arrangements and exhibit fundamentally different failure behavior. Instead of abrupt delamination, they develop diffuse, helicoidal matrix cracking that spreads stress and dissipates energy, resulting in low notch sensitivity despite reduced 0 ° fiber content. Further research [10] showed that, unlike cross-ply laminates which suffer from brittle or pull-out failure depending on fiber angle, Bouligand layups maintain more stable, spiral fracture patterns across varying off-axis angles. This leads to more balanced strength and improved structural reliability in notched and multi-axial loading scenarios, making Bouligand designs well-suited for advanced load-bearing applications.

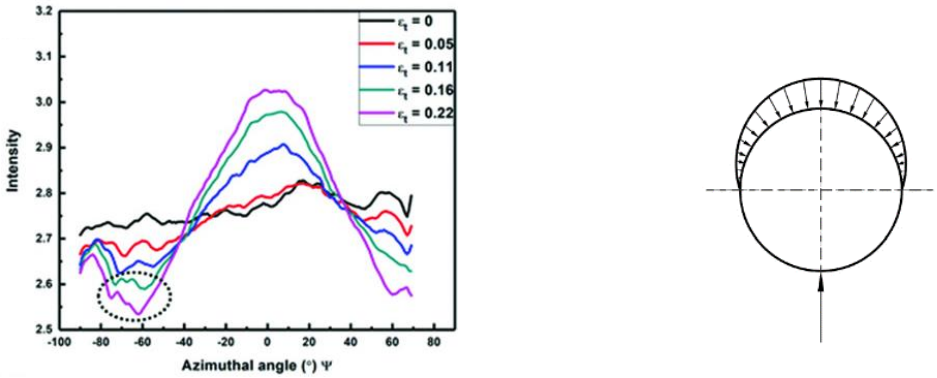

Figure 1. Diffraction intensity versus azimuthal angle of fish scales [1] (left) and typical stress state in bearing laminates (right) [11]

In addition to the fully developed Bouligand structures, nature has also produced structures during evolution that are specifically designed for certain load cases. A remarkable example of this can be found in coelacanth fish scales. In an unloaded state, the tissue of the fish scale shows a so-called double-twisted Bouligand structure. As [1] was able to demonstrate using in-situ synchrotron SAXS during tensile tests, the fibrils orientate themselves in the direction of the mechanical stress. The orientation of the fibrils under load application is shown in Figure 1. (left). The in-situ synchrotron SAXS measurements indicate that the fish scale forms an oriented Bouligand structure, hereafter called partial Bouligand structure, under uniaxial tensile stress. This structure extends over an angular range of ±60 °, with the strongest fibril alignment occurring in the range of ±40 ° compared to the unloaded scale. A comparison of the fibril

orientation under uniaxial tensile load with the stress curve of a composite bolted join shown in Figure 1. (right) shows similarity.
In this study, the partial Bouligand structure of the coelacanth is replicated for engineering applications, fiber angles of ±60 ° and ±40 °, as observed in fish scale, were combined with the traditional Load-Introduction (LI), layup commonly used in bolted-join and open-hole composite laminates. The conventional LI layup, established in the aviation industry and widely applied to promote bearing failure while suppressing other failure modes, serves as a benchmark for comparison in this study, with the following layer configurations [2, 3]:

30_LI: 30 gsm: $[45, 0, -45, 0, 90, 0, 45, 0, -45, 0]_{6s}$
60_LI: 60 gsm: $[45, 0, -45, 0, 90, 0, 45, 0, -45, 0]_{3s}$

An analytical optimization of the LI layup was performed to match both the stiffness characteristics of the LI configuration and the biologically inspired fiber angles. On this basis, a stiffness optimization was carried out using classical laminate theory in order to develop a partial Bouligand structure, hereafter called B, $\left[\sum_{k=0}^{i}(\alpha - k \cdot \theta)\right]_S$ with comparable stiffness properties. A schematic representation of a partial Bouligand structure is shown in Figure 2.

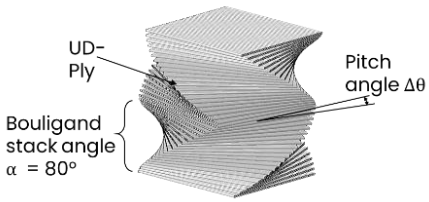

Figure 2. Schematic representation of a partial Bouligand structure

Two different optimization approaches were selected. The first approach focused on optimizing the elastic properties A_{11} and A_{22}. The corresponding objective function was defined as follows:

$$f(\alpha, \theta) = \left|\frac{A_{11\_BI}}{A_{11\_LI}}\right| + \left|\frac{A_{22\_BI}}{A_{22\_LI}}\right| \quad (1)$$

The following layup configurations were derived based on the minimization function and show a close correspondence to the ±60° oriented fibrillar structure observed in the fish scale:

30_BI_1: 30 gsm: $\left[\sum_{k=0}^{59}(64.9° - k \cdot 2.2°)\right]_S$
60_BI_1: 60 gsm: $\left[\sum_{k=0}^{29}(63.8° - k \cdot 4.4°)\right]_S$

The second optimisation approach aimed to optimise the stiffness in the main load direction. For this purpose, the effective stiffness E_{11} was considered according to the relationship $E_{11} = \frac{1}{h} \cdot \left(A_{11} - \frac{A_{12}^2}{A_{22}}\right)$ and the following minimisation function was applied:

$$f(\alpha, \theta) = |E_{11\_BI} - E_{11\_LI}| \quad (2)$$

Based on this minimization function, the following layup configuration was obtained that aligns closely with the highly oriented fibril angle ±40 ° observed in the fish scale:

$$60\_BI\_2 \qquad 60 \text{ gsm: } \left[\sum_{k=0}^{28}(40.5° - k \cdot 2.9°)\right]_S$$

2. Materials and methods

In the present study, unidirectional prepregs with two different fiber areal weights (30 gsm and 60 gsm) were manufactured by North Thin Ply Technology (NTPT) using Toray S700SC-12K-60E carbon fibers and NTPT ThinPreg 402 epoxy resin.

To evaluate the mechanical strength and damage tolerance of the Bouligand structures compared to conventional layups, experimental tests were conducted following ASTM D3039 [12] for unnotched tension (UNT) and ASTM D5961 Procedure A (Double Shear Test) [13] for bearing performance. Prior to testing, all specimens were conditioned for 48 hours at 40 °C under vacuum to ensure consistent material properties. UNT tests were performed using a ZwickRoell Z100 universal testing machine (maximum load 100 kN) equipped with hydraulic grips. Bearing tests were conducted using a double shear clevis fixture and a ZwickRoell Z400 machine (max. load 400 kN) with mechanical wedge grips. Load was applied to the specimen through a pin installed in the clevis using a torque of 6 Nm. A steel washer (inner diameter 6.3 mm, outer diameter 12 mm) was used to transmit transverse compressive force around the hole periphery. Strain measurements were apprehended using a 4M Digital Image Correlation (DIC) system by GOM GmbH. A pattern was applied to the surface of the specimen and bearing fixture to enable strain tracking. Data analysis was conducted using ARAMIS Professional software 2016, also provided by GOM GmbH. All tests were carried out under standard laboratory conditions of 20 °C and 50 % relative humidity.

3. Results

3.1. Unnotched Tension

Table 1. contains the test data of the UNT experiment. The results demonstrate that the Bio-Inspired (BI) exhibit significantly lower strength and fracture strain compared to the LI structures. This effect is consistent with the significantly lower content of 0 ° plies in loading direction. An equal stiffness can be observed between the LI structures and the 60_BI_2 structure, which was optimized to E_{11}. In general, the LI structures exhibited spontaneous brittle failure due to fiber breakage, whereas the BI showed a gradual fiber-matrix failure along a helical crack path starting in plies oriented at ±α. This type of failure in Bouligand structures has been reported in several publications [9]. Based on the test data, no significant influence of the ply thickness can be determined.

Table 1. Theoretical and experimental mechanical properties of UNT

Layup	*Calc. Young's modulus* (GPa)	*Young's modulus* (GPa)	*Tensile strength* (MPa)	*Fracture strain* (%)
30_LI	79,78	69,07	1.224,54	1.65
60_LI	77,38	69,94	1.299,98	1.74
30_BI_1	60,65	55,04	427,39	0.79
60_BI_1	58,91	52,15	413,83	0.80
60_BI_2	80,02	69,03	519,61	0.77

3.2.Load-Bearing

In the following section, the results of the bearing experiments will be displayed and discussed. Figure 3. illustrates the experimental data of the bearing tests, showing the ultimate bearing strength as a function of the bearing strain. From the Figure 3. and Table 2., it is evident that the LI structures exhibit the highest bearing strengths. Additionally, there is a notable increase of 17.8 % in ultimate bearing strength when comparing the 30_LI to the 60_LI specimens. This improvement is attributed to the increased thickness of the laminate, as both configurations share an identical layup. Furthermore, it can be observed that the BI show lower bearing strengths overall. Specifically, the 60_BI_2 structure has the lowest bearing strength overall. The 30_BI_1 and 60_BI_1 samples demonstrate approximately 44.8 % higher strengths compared to the 60_BI_2 structure. However, these values are still 28.3 % lower than those of the 60_LI and 15.5 % lower than the 30_LI specimens.

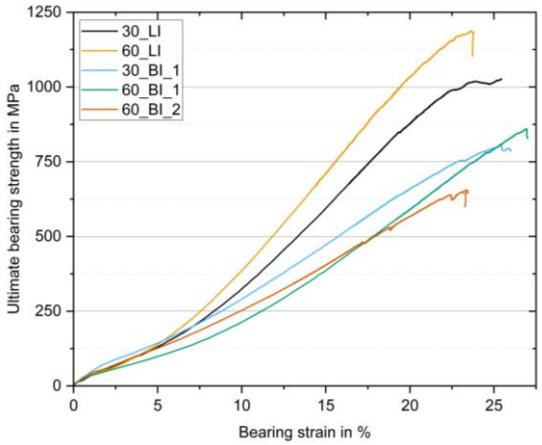

Figure 3. Stress-strain-diagram bearing

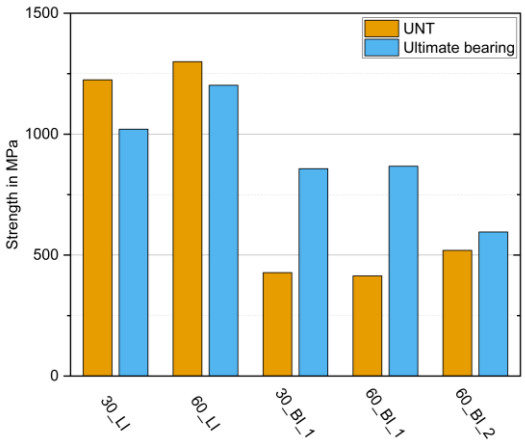

Figure 4. UNT and bearing strength

Table 2. Ultimate bearing strength and notch sensitivity factor

Layup	*Ultimate bearing strength* (MPa)	*Ultimate bearing strength / tensile strength*
30_LI	1.020,44	0,83
60_LI	1.202,21	0,92
30_BI_1	857,16	2,01
60_BI_1	867,68	2,10
60_BI_2	595,68	1,15

Comparing the tensile strength of the unnotched tension specimens with the ultimate bearing strength shown in Figure 4. reveals an intriguing correlation. The BI, particularly those with larger stacking angles, exhibit a significantly higher ultimate bearing strength relative to their tensile strength. Specifically, the 30_BI_1 and 60_BI_1 configurations demonstrate an increase in ultimate bearing strength of 101 % and 110 %, respectively, compared to their tensile strength (see Table 2.). In contrast, the LI structures show a decrease in stress under bearing conditions. This enhancement can be attributed to the fact that the BI with larger stacking angles better accommodate the stress distribution generated around the bolt, as the fiber arrangement

more closely follows the stress pattern shown in Figure 1. (right).
Figure 5. shows the representative fracture patterns of the various laminate structures, with the note that the layer thickness has no influence on the failure mode. The fracture pattern of the LI structures shows a mixed mode failure between shear out and bearing failure concentrated around the bolt in loading direction and therefore behaves contrary to expectations. In the BI, the fracture patterns vary significantly. In both configurations, 30_BI_1 and 60_BI_1, a combination of the intended bearing failure and a failure mode that is not classified according to the standard, characterized by helical cracks, occur. Continuous failure through helical cracks in Bouligand structures has been described in the literature [9] before, but never in connection with bearing failures. For the 60_BI_2 configuration, failure was predominantly governed by helicoidal cracking, with cracks propagating toward the top of the specimen. Based on these observations, it can be hypothesized that with decreasing stack angle in combination with smaller pitch angle, the helical crack growths further towards the edges of the specimens.

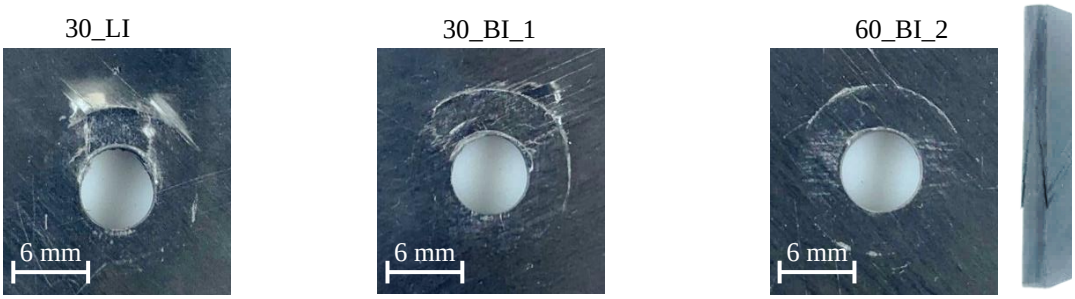

Figure 5. Fracture patterns of bearing specimens

4. Conclusion

This study highlights the significant potential of translating biological structural principles, which have been continuously optimized through evolution to withstand specific load conditions, into technical engineering applications. The comparison between the Load Introduction and Bouligand layups provided valuable insights into their mechanical performance characteristics. While the unnotched tension Bouligand specimens exhibited lower tensile strength relative to Load Introduction layups, the 60_BI_2 partial Bouligand layup reached comparable stiffness values. Moreover, the ultimate bearing strength of the Bouligand structures, particularly those with larger stacking angles, surpassed that of the UNT specimens by 200 %. This remarkable enhancement in bearing capacity is indicative of the superior load distribution capabilities inherent to the Bouligand architecture, which more effectively mitigates stress concentrations around fastener holes. Overall, these findings demonstrate that bioinspired laminate configurations, derived from naturally occurring fiber arrangements, offer promising avenues for the development of advanced composite materials with tailored mechanical properties for engineering applications where bearing strength and damage tolerance are critical.

Acknowledgments

The authors gratefully acknowledge the support of the DAAD (Project: 57710630) and the German Research Foundation (DFG, project number 513556749) for funding this project.

References

[1] H. Quan, W. Yang, E. Schaible, R. O. Ritchie, M. A. Meyers. Novel Defense Mechanisms in the Armor of the Scales of the "Living Fossil" Coelacanth Fish. *Adv. Funct. Mater.*, Volume 28(46), Art.-Nr. 1804237, 2018.
[2] M. Shan, R. Zhang, F. Liu, L. Zhao. A characteristic curve including hygrothermal effects for predicting the failure of composite multi-bolt joints. *Composites Communications*, Volume 36, Art.-Nr. 101384, 2022.
[3] S. S. Naarayan, D.V.T.G. P. Kumar, S. Chandra. Implication of unequal rivet load distribution in the failures and damage tolerant design of metal and composite civil aircraft riveted lap joints. *Engineering Failure Analysis*, Volume 16: 2255-2273, 2009.
[4] S. Sihn, R. Y. Kim, K. Kawabe, and S. W. Tsai. Experimental studies of thin-ply laminated composites. *Composites Science and Technology*, Volume 67(6):996–1008, 2007.
[5] A. Arteiro, C. Furtado, G. Catalanotti, P. Linde, and P. P. Camanho. Thin-ply polymer composite materials: A review. *Composites Part A: Applied Science and Manufacturing*, Volume 132, Art.-Nr. 105777, 2020.
[6] R. Amacher, J. Cugnoni, J. Botsis, L. Sorensen, W. Smith, and C. Dransfeld. Thin ply composites: Experimental characterization and modeling of size-effects. *Composites Science and Technology*, Volume 101:121–132, 2014.
[7] J. Cugnoni, R. Amacher, S. Kohler, J. Brunner, E. Kramer, C. Dransfeld, W. Smith, K. Scobbie, L. Sorensen, and J. Botsis. Towards aerospace grade thin-ply composites: Effect of ply thickness, fibre, matrix and interlayer toughening on strength and damage tolerance. *Composites Science and Technology*, Volume 168:467–477, 2018.
[8] L. Mencattelli, S. T. Pinho. Ultra-thin-ply CFRP Bouligand bio-inspired structures with enhanced load-bearing capacity, delayed catastrophic failure and high energy dissipation capability. *Composites Part A: Ap-plied Science and Manufacturing*, Volume 129, Art.-Nr. 105655, 2020.
[9] J. Körbelin, P. Goralski, B. Kötter, F. Bittner, H.-J. Endres, B. Fiedler. Damage tolerance and notch sensitivity of bio-inspired thin-ply Bouligand structures. *Composites Part C: Open Access*, Volume 5, Art.-Nr. 100146, 2021.
[10] H. Luo, H. Wang, Z. Zhao, H. Xue, and Y. Li. Experimental and numerical investigation on the failure behavior of Bouligand laminates under off-axis open-hole tensile loading. *Composite Structures*, Volume 313, Art.-Nr. 116932, 2023.
[11] H. Huang, M. Li, W. Zhang, Y. Yuan. Seismic behavior of a friction-type artificial plastic hinge for the precast beam–column connection. *Archiv.Civ.Mech.Eng*, Volume 22, Art.-Nr. 201, 2022.
[12] ASTM D3039-00. *Test Method for Tensile Properties of Polymer Matrix Composite Materials*. ASTM International, West Conshohocken, 2017.
[13] ASTM D5961-01. *Test Method for Bearing Response of Polymer Matrix Composite Laminates*. ASTM International, West Conshohocken, 2017.